BJ Biomolecules

Biochem. J. (2014) **462**, 499–511 (Printed in Great Britain) doi:10.1042/BJ20140266

online data

Crystal structures and functional studies clarify substrate selectivity and catalytic residues for the unique orphan enzyme *N*-acetyl-D-mannosamine dehydrogenase

Agustín SOLA-CARVAJAL*[1], Fernando GIL-ORTIZ†‡[1], Francisco GARCÍA-CARMONA*, Vicente RUBIO†[2] and Álvaro SÁNCHEZ-FERRER*§[2]

*Department of Biochemistry and Molecular Biology-A, Faculty of Biology, Regional Campus of International Excellence "*Campus Mare Nostrum*", University of Murcia, Campus Espinardo, E-30100 Murcia, Spain

†Instituto de Biomedicina de Valencia-Consejo Superior de Investigaciones Científicas (IBV-CSIC) and Centro de Investigación Biomédica en Red de Enfermedades Raras (CIBERER-ISCIII), Valencia, Spain

‡CELLS-ALBA Synchrotron Light Source, 08290 Barcelona, Spain

§Murcia Biomedical Research Institute (IMIB-Arrixaca), 30120 Murcia, Spain

NAMDH (*N*-acetyl-D-mannosamine dehydrogenase), from the soil bacteroidete *Flavobacterium* sp. 141-8, catalyses a rare NAD^+-dependent oxidation of ManNAc (*N*-acetyl-D-mannosamine) into *N*-acetylmannosamino-lactone, which spontaneously hydrolyses into *N*-acetylmannosaminic acid. NAMDH belongs to the SDR (short-chain dehydrogenase/reductase) superfamily and is the only NAMDH characterized to date. Thorough functional, stability, site-directed mutagenesis and crystallographic studies have been carried out to understand better the structural and biochemical aspects of this unique enzyme. NAMDH exhibited a remarkable alkaline pH optimum (pH 9.4) with a high thermal stability in glycine buffer ($T_m = 64\,°C$) and a strict selectivity towards ManNAc and NAD^+. Crystal structures of ligand-free and ManNAc- and NAD^+-bound enzyme forms revealed a compact homotetramer having point 222 symmetry, formed by subunits presenting the characteristic SDR $\alpha_3\beta_7\alpha_3$ sandwich fold. A highly developed C-terminal tail used as a latch connecting nearby subunits stabilizes the tetramer. A dense network of polar interactions with the substrate including the encasement of its acetamido group in a specific binding pocket and the hydrogen binding of the sugar 4OH atom ensure specificity for ManNAc. The NAMDH–substrate complexes and site-directed mutagenesis studies identify the catalytic tetrad and provide useful traits for identifying new NAMDH sequences.

Key words: *Flavobacterium* sp. 141-8, *N*-acetyl-D-mannosamine, *N*-acetyl-D-mannosamine dehydrogenase, short-chain dehydrogenase/reductase, sialic acid, substrate selectivity.

INTRODUCTION

ManNAc (*N*-acetyl-D-mannosamine) is a common amino sugar that is part of the biosynthetic pathway of sialic acids, which are the usual components of glycoproteins and gangliosides in animals [1]. The most common form of sialic acid, Neu5Ac (*N*-acetylneuraminic acid) is found as such in body fluids [2], and is considered a biomarker for some tumoral [3] and inflammatory [4] states, rendering its determination in serum important [2,5]. In addition, Neu5Ac is present in some bacteria that live in close association with animals (deuterostomes), as a part of capsular polysialic acid polymers that, by mimicking animal components, can be important elements in the pathogenicity of these bacteria [6–8].

Being a widespread biochemical component, sialic acid is scavenged (Figure 1) by many bacteria from the surrounding environment [8–10]. Thus bacteria use sialidases (Figure 1A) to cleave sialic acid from sialo-glycoconjugates and then they utilize Neu5Ac aldolase to split Neu5Ac to pyruvate and ManNAc. Pyruvate can be used in a number of fermentative processes such as lactic, homolactic and alcoholic fermentation, whereas ManNAc is first converted into *N*-acetyl-D-glucosamine-6-phosphate by a combination of phosphorylation and epimerization, and then this last phosphorylated acetyl amino sugar is deacylated and deaminated, yielding fructose 1,6-bisphosphate, which is used by the glycolytic route of the bacteria (Figure 1A).

Although the conversion into fructose 1,6-bisphosphate is the usual process of sialic acid catabolism in bacteria, which have variants depending on whether the epimerization or the phosphorylation step occurs first [11], a soil bacterium, *Flavobacterium* sp. 141-8, isolated because of its ability to grow on ManNAc as the sole carbon source [12], was found to oxidize sialic acid (Figures 1A and 1B) by a unique dehydrogenase (EC 1.1.1.233), NAMDH (*N*-acyl-D-mannosamine dehydrogenase), to *N*-acetylmannosamino-lactone, with subsequent spontaneous hydrolysis of the lactone to yield *N*-acetylmannosaminic acid [12] (Figure 1B). In line with the very limited biological information existing on *Flavobacterium* sp. 141-8 (contained in U.S. Pat. 4,960,701) [13], the physiological role of this enzyme remains unclarified, not having been found in any other micro-organism. However, a commercial application for NAMDH has been found.

Abbreviations: AldT, aldohexose dehydrogenase; CCD, charge-coupled device; C-tail, C-terminal tail; FspNAMDH, NAMDH from *Flavobacterium* sp. 141-8; 3β/17β-HSD, 3β/17β-hydroxysteroid dehydrogenase; ManNAc, *N*-acetyl-D-mannosamine; NAMDH, *N*-acetyl-D-mannosamine dehydrogenase; Neu5Ac, *N*-acetylneuraminic acid; RsGDH, *Rhodobacter sphaeroides* galactitol dehydrogenase; SDR, short-chain dehydrogenase/reductase; TLS, translation–libration–screw–rotation.

[1] These authors contributed equally to this work.

[2] Correspondence may be addressed to either of these authors (rubio@ibv.csic.es or alvaro@um.es).

The co-ordinates and structure factors for the FspNAMDH-apo, FspNAMDH–ManNAc and FspNAMDH–NAD crystal structures have been deposited in the PDB under codes 4CR6, 4CR7 and 4CR8 respectively.

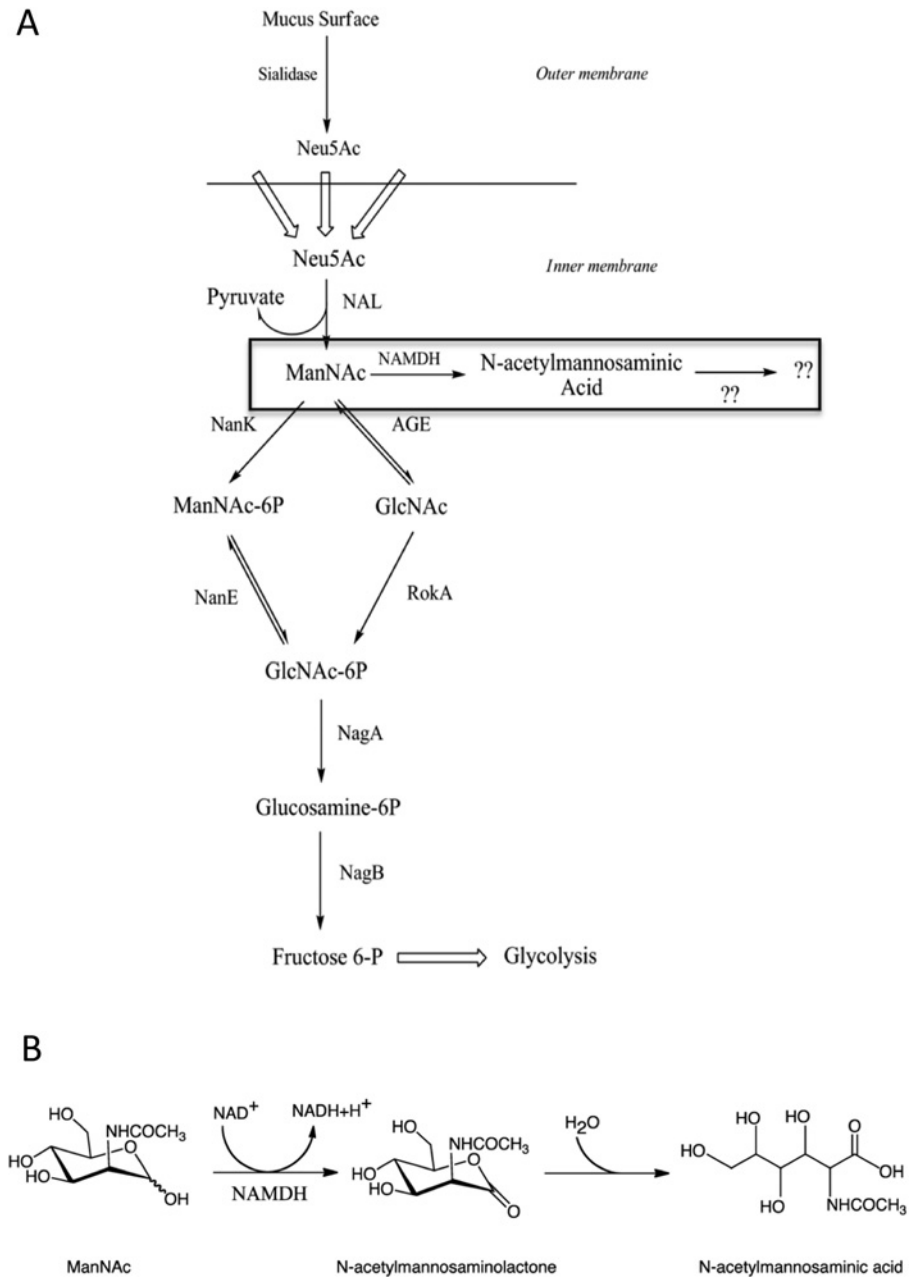

Figure 1 Sialic acid catabolism and the FspNAMDH reaction

(**A**) Catabolism of sialic acid (Neu5Ac) in bacteria. The reaction catalysed by NAMDH is boxed. AGE, N-acyl-D-mannosamine 2-epimerase; ManNAc-6P, *N*-acetyl-D-mannosamine 6-phosphate; NagA, N-acetylglucosamine 6-phosphate deacetylase; NagB, glucosamine 6-phosphate deaminase; NAL, N-acetylneuraminic acid aldolase; NanE, N-acetyl-D-glucosamine 2-epimerase; NanK, N-acetylmannosamine kinase; RokA, hexokinase. (**B**) FspNAMDH uses NAD^+ to oxidize ManNAc to *N*-acetylmannosamino lactone, which is then spontaneously hydrolysed to *N*-acetylmannosaminic acid.

By coupling the Neu5Ac aldolase and NAMDH reactions, sialic acid can be assayed in fluids by simply following NAD reduction [5]. This led to the early production with this purpose of FspNAMDH (NAMDH from *Flavobacterium* sp. 141-8) [12], and, later on, to the cloning of the gene from this micro-organism that encodes NAMDH and the recombinant production of this enzyme [14], which was sold commercially as a part of a sialic acid assay kit.

Although NAMDH had been used widely, little was known about this enzyme [12,14]. Our interest in NAMDH was spurred by our recent studies [15] on another enzyme of biotechnological value, D-sorbitol dehydrogenase (used for sorbitol assay in food, pharmaceutical and cosmetic preparations). We were surprised to find that the putative sequence for this enzyme from *Rhodobacter capsulatus* SB1003 appeared in the UniProtKB database (http://www.uniprot.org) under two different accession numbers (D5AUY1 and O68112) and annotated as both a sorbitol dehydrogenase and NAMDH. When we cloned and expressed the *R. capsulatus* gene (NCBI 9004849) for this putative protein [15], the purified protein product was clearly a sorbitol dehydrogenase with no NAMDH activity. If the UniProtKB database is queried with the NAMDH EC number 1.1.1.233,

14 entries appear, which include the genuine NAMDH from *Flavobacterium* sp. 141-8 (FspNAMDH), but also *R. capsulatus* sorbitol dehydrogenase and other putative proteins of different lengths, some of them with much longer sequences than that of the experimentally demonstrated FspNAMDH, rendering it difficult to ascertain which are the key characteristics that could allow the annotation with a high degree of certainty of a sequence as truly corresponding to NAMDH. Since structural determination can be a way to define these key characteristics, helping to identify sequence motifs associated with a given function, we decided to determine the crystal structure of the only known genuine FspNAMDH.

We report the results of these studies, which are not just crystallographic, since they also include functional and site-directed mutagenesis studies. The structure of FspNAMDH confirms this enzyme as a member of the SDR (short-chain dehydrogenase/reductase) family [16]. This large functionally convergent protein family is nucleated by the common structural trait of sharing a dinucleotide-binding motif. However, the modest to low sequence identity (15–30 %) among the members of this family [17] and the presence in these enzymes of a highly variable C-terminal segment hosting the site for the non-dinucleotide substrate [18,19] has resulted in great diversity of specificities and even different activities and reactional mechanisms within the family, which not only includes dehydrogenases/reductases, but also lyases and some isomerases [20].

Our crystal structures of FspNAMDH in a free form or bound to ManNAc or NAD^+, at respective resolutions of 1.9 Å, 2.15 Å and 2.2 Å (1 Å = 0.1 nm), reveal a homotetrameric 222 point group architecture with subunits conforming to the SDR family fold. The structures clarify how the enzyme can select for ManNAc. Structural analysis and site-directed mutagenesis studies corroborate that Asn^{119}, Ser^{153}, Tyr^{166} and Lys^{170} constitute the catalytic tetrad which is typical of the SDR family [16,21]. A water-rich pocket is identified as a proton reservoir/acceptor, allowing proton transfer to the solvent during catalysis. By being clamped between two elements of another subunit, the highly developed C-tail (C-terminal tail) plays a key role in interlinking different subunits and stabilizing the tetramer. The comparison of the structures of the ligand-free and substrate-containing structures fails to reveal significant conformational changes upon ManNAc or NAD^+ binding.

EXPERIMENTAL

Cloning, expression and protein purification

Molecular biology techniques were carried out as described [22]. The FspNAMDH gene (GenBank accession number BAA14346.1) was cloned from genomic DNA (obtained from an overnight culture in Bouillon medium) of *Flavobacterium* sp. 148-1 cells (provided by the International Patent Organism Depositary, Japan) by PCR. For this PCR cloning we used a high fidelity thermostable DNA polymerase (PfuUltra II, Stratagene); the respective forward and reverse oligonucleotides were 5′-CG-GC*GAATTC*ATGACAACAGCAGGCGTTTC-3′ and 5′-CTAC-*CTCGAG*TCAGCGTCGGCCTTCC-3′, which contained restriction sites (highlighted in italics) for EcoRI (forward primer) and XhoI (reverse primer) for directional insertion of the product in the corresponding sites of pET28a (Novagen). The PCR mixture was supplemented with 0.125 M betaine and 5 % dimethylsulfoxide (because of the 77 % GC content of the gene). The PCR product was inserted into pET28a (Novagen), yielding the plasmid pFspNAMDH, encoding the protein with an N-terminal 36-residue His_6 tag. This plasmid, isolated from electrotransformed *Escherichia coli* DH5α electrocompetent cells (Novagen), was used for transformation of *E. coli* Rosetta 2(DE3) cells (Novagen). Protein expression and purification were carried out as described previously for BoAGE2 [22], except for the utilization of a 50 kDa cut-off membrane in the ultrafiltration step, and the use in the next step of column chromatography on a Ni^{2+}-loaded HiPrep IMAC 16/10 FF column (GE Life Sciences) connected to an Äkta Prime FPLC system (GE Life Sciences). The fractions containing the pure protein (purity monitored by SDS/PAGE [23]) were concentrated by centrifugal ultrafiltration to ∼6 mg/ml (Bradford assay [24], using a commercial reagent from Bio-Rad Laboratories and BSA as a standard).

Site-directed mutagenesis

Six single mutants (N119A, N119S, S153T, Y166N, Y166Q and K170R) were prepared by the overlapping extension method [25] using pFspNAMDH as the template and appropriate mutagenic oligonucleotides (Supplementary Table S1 at http://www.biochemj.org/bj/462/bj4620499add.htm). PCR products were digested with DpnI, and transformed in *E. coli* DH5α electrocompetent cells. The presence of the mutations and the absence of unwanted changes were confirmed by DNA sequencing. Production of the mutant proteins in Rosetta cells and their purification were as for the wild-type enzyme.

Enzyme activity assays

NAMDH activity was assayed [12] as NAD^+ reduction by monitoring the increase in the absorbance at 340 nm in 1 ml of assay mixtures at 37 °C containing 50 mM glycine, pH 9.5, 3 mM NAD^+ and 5 mM ManNAc. For determination of K_m values for the two substrates, one of the substrates was kept at the concentration used in the standard assay and the second substrate was varied in an appropriate range to approach saturation. Results were fitted to hyperbolic kinetics using GraphPad Prism.

Crystallization and data collection

The sparse matrix vapour diffusion sampling procedure [26] was used for screening crystallization conditions at 21 °C in sitting drops of 0.4 μl of reservoir fluid and 0.4 μl of 5.5 mg/ml FspNAMDH in 0.02 M Tris/HCl, pH 8.0, alone or supplemented with 10 mM ManNAc or 5 mM NAD^+. The best FspNAMDH crystals prepared without ligands (FspNAMDH-apo) or with ManNAc (FspNAMDH–ManNAc) had a cubic shape (0.2 mm maximal dimension) and grew using 0.1 M Hepes, pH 7.5, and 30 % (w/v) PEG 300 as a crystallization solution. Both crystals were frozen directly from the drop. The crystal prepared in the presence of NAD^+ (FspNAMDH–NAD) had a plate shape, grew in 8 % (w/v) PEG 4000 and was frozen in liquid nitrogen after passage through crystallization solution enriched with 30 % (w/v) PEG 400. FspNAMDH-apo and FspNAMDH–ManNAc crystals were diffracted at 100 K (Oxford Cryosystems) at the ESRF (European Synchrotron Radiation Facility) synchrotron (Grenoble) (Table 1), using a 225 mm MarMOSAIC CCD (charge-coupled-device camera) detector and an ADSC Quantum 210r CCD detector respectively. Crystals of the NAD^+ complex were diffracted at the Diamond Light Source Synchrotron (Harwell, Oxfordshire), using an ADSC Quantum Q315r CCD detector. Data was processed with MOSFLM or XDS, SCALA and TRUNCATE [27,28] (Table 1). Ligand-free and ManNAc-containing crystals had triclinic cells (space group *P*1) (Table 1) with one and four homotetramers in the asymmetric unit respectively at 44 % solvent content. The FspNAMDH–NAD

Table 1 Data collection and refinement statistics

Values in parenthesis are data for the highest resolution shell. $R_{sym} = \Sigma|I - <I>|/\Sigma I$, where I is the observed intensity and $<I>$ is the average intensity of multiple observations of symmetry-related reflections. R-factor $= \Sigma_{hkl}||F_{obs}| - |F_{calc}||/\Sigma_{hkl}|F_{obs}|$, where F_{obs} and F_{calc} are the observed and calculated structure factors respectively. The Ramachandran plots were calculated using PROCHECK.

Parameter	Native	ManNAc complex	NAD^+ complex
Data collection			
Beamline	ID23-2 (ESRF)	ID23-1 (ESRF)	I24 (DLS)
Wavelength (Å)	0.9393	0.9724	0.9796
Space group	*P*1	*P*1	*C*2
Unit cell			
a, b, c (Å)	59.3, 59.1, 74.2	99.4, 100.1, 111.6	158.9, 146.8, 90.4
α, β, γ (°)	81.1, 73.3, 79.3	67.4, 89.8, 72.5	90.0, 115.3, 90.0
Resolution range (Å)	50.00–1.90 (2.00–1.90)	57.49–2.15 (2.27–2.15)	50.00–2.20 (2.32–2.20)
Reflections (total/ unique)	128784/67168	507562/199836	357924/94228
$I/\sigma I$	6.2 (3.9)	5.2 (1.7)	5.1 (1.9)
R_{sym}(%)	6.4 (16.9)	9.3 (35.8)	14.0 (39.3)
Completeness (%)	90.5 (92.7)	96.9 (97.8)	99.4 (99.2)
Refinement			
Resolution range (Å)	12–1.90	15–2.15	20–2.20
Reflections (work/test)	63579/3360	189715/10032	89504/4723
R-factor (work/test) (%)	20.9/22.8	20.1/23.1	22.19/25.3
Average B-factors (Å^2)			
Protein atoms	26.71	26.84	10.64
NAM	–	44.64	–
Mannose	39.9	28.70	–
NAD^+	–	–	15.71
Water	16.59	27.49	10.77
Number of:			
Polypeptide chains	4	16	8
Protein atoms	7180	29146	14733
ManNAc molecules	–	16	–
Mannose molecules	2	4	–
NAD^+ molecules	–	–	8
Water molecules	213	811	645
RMSD bond (Å)	0.015	0.012	0.012
RMSD angle (°)	1.35	1.33	1.41
Ramachandran plot			
Most favoured (%)	91.4	90.3	91.8
Additional allowed (%)	8.6	9.7	8.2
Generously allowed (%)	0.0	0.0	0.0
Disallowed (%)	0.0	0.0	0.0

crystal had a monoclinic cell (space group *C*2) with two tetramers in the asymmetric unit and 43 % solvent content.

Structure solution and refinement

Table 1 summarizes refinement and model data. Phases were determined by molecular replacement with MOLREP [27] using a polyalanine model of a subunit of TT0321 from *Thermus thermophilus* HB8 (PDB code 2D1Y; 34 % sequence identity with FspNAMDH), a hypothetical oxidoreductase having a Rossmann NAD(P) fold, as a search model for the FspNAMDH-apo crystal. The structure obtained (see below) allowed molecular replacement in the crystals with ligands. Initial model building and map improvement were performed using the program ARP/wARP [27]. Rigid body refinement was performed stepwise with increased resolution, and it was followed by automated refinement using REFMAC5 [27], alternating with graphic manual model adjustment sessions using COOT [29]. Electron density from the resulting difference maps was interpreted, building the protein model except for residues 1–9, which lack electron density. B-factors and positional non-crystallographic symmetry restraints were used and gradually released as refinement progressed. All of the diffraction data were used throughout the refinement process except the 5 % of randomly selected data for calculating R_{free}. TLS (translation–libration–screw-rotation) was applied in the last steps of refinement with the TLSMD server for definition of the TLS groups [30]. The final models at 1.90 Å, 2.15 Å and 2.2 Å (FspNAMDH-apo, FspNAMDH–ManNAc and FspNAMDH–NAD respectively) exhibited excellent R_{factor}/R_{free} values (Table 1), including in the asymmetric unit one, four and two homotetramers respectively. Non-protein electron density was found in the active centre of each subunit, which fitted best a bound ManNAc or the ADP moiety of NAD^+ in the FspNAMDH–ManNAc and FspNAMDH–NAD crystals respectively. Also, electron density compatible with a mannose molecule was found at the intersubunit interface of the tetramer, coincident with the 4-fold axis in the FspNAMDH-apo and FspNAMDH–ManNAc complexes (Table 1). Structure analysis with PROCHECK yielded excellent stereochemistry for both models [31] (Table 1).

A superimposition of structures and RMSD calculation were carried out with the SSM option of COOT using default parameters [29,32]. The Figures were drawn using PyMOL (http://www.pymol.org) and ESPript [33].

Other techniques

Thermal unfolding of 1 μg of enzyme was followed with a real-time PCR instrument by monitoring Sypro Orange (Molecular Probes) fluorescence with increasing temperature (ramp, 1 °C/min) according to the methods discussed previously [34,35], in a mixture containing 50 mM of the indicated buffer.

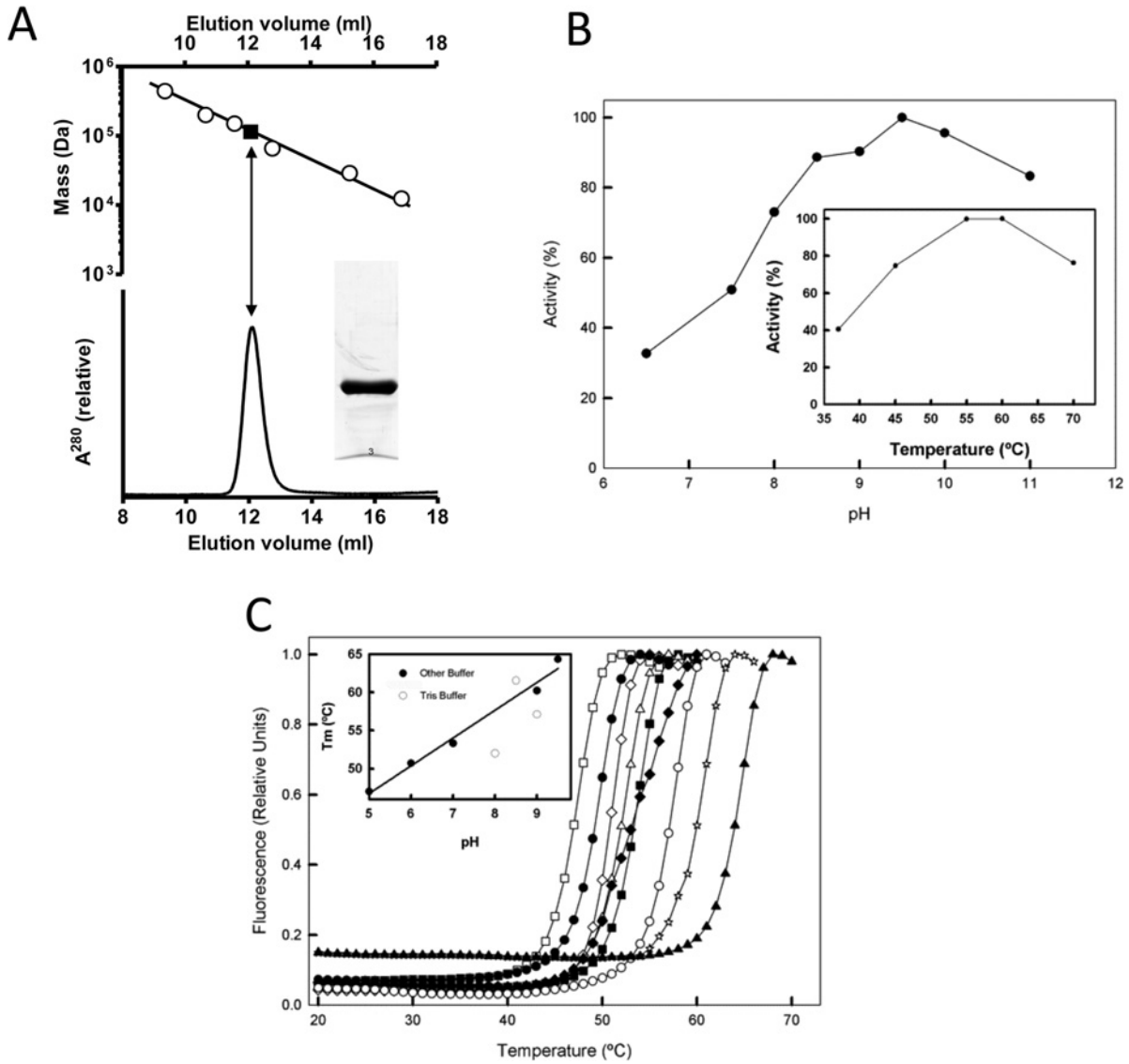

Figure 2 Properties of FspNAMDH

(**A**) Size-exclusion chromatography of pure (shown in the inset, by SDS/PAGE) FspNAMDH. The bottom panel illustrates the optical absorption (280 nm) of the effluent. The top panel illustrates a semi-logarithmic plot of molecular mass against elution volume. Open circles correspond to the following protein standards (mass is given in kDa in parentheses): cytochrome *c* (12.4), carbonic anhydrase (29), BSA (66.4), alcohol dehydrogenase (150), β-amylase (200) and apoferritin (440). The closed square plots the elution volume of the main peak against the sequence-deduced mass for a tetramer (124.8 kDa). (**B**) Dependence of the enzyme activity on pH (main panel) and temperature (inset, assayed at pH 9.5). The buffers used (50 mM) were sodium phosphate (pH 6.5–7.5), Tris/HCl (pH 8.0–9.0) and glycine (pH 9.5–11). (**C**) FspNAMDH thermal unfolding monitored by the increase in Sypro Orange fluorescence using the thermofluor approach. The buffer (50 mM) used was: (□) sodium acetate, pH 5.0; (●) none; (◇ and ■) sodium phosphate pH 6.0 and 7.0 respectively; (△, ◆ and ○) Tris/HCl pH 8.0, 8.5 or 9.0 respectively; (☆ and ▲), glycine pH 9.0 or 9.5 respectively. Inset: T_m (temperature at which the increase in fluorescence is 50 % of the maximum increase) as a function of pH.

Gel filtration (Superdex 200 10/300 GL, GE Life Sciences) was used to confirm the homogeneity and to determine the molecular mass of the purified enzyme, in 0.05 M Tris/HCl, pH 7.5, containing 0.15 M NaCl [35].

Precise subunit molecular mass determination was carried out using LC-ESI–MS, using an HP/1100 LC/MSD Ion Trap System (Agilent Technologies) and Ion Trap software (version 3.2) [35].

RESULTS AND DISCUSSION

Enzyme expression, purification and characterization

The N-terminally His_6-tagged protein product of the cloned FspNAMDH gene (GenBank accession number BAA14346.1) was produced in abundance (∼900 mg/l of culture), in homogeneous form (Figure 2A, inset) and ∼80 % yield, after a two-step purification procedure. The enzyme was a tetramer as judged from its gel-filtration elution as a peak (Figure 2A) (124.8 kDa, for a subunit mass of 31.2 kDa, corroborated by MS). The enzyme was highly active (specific activity at pH 9.5 and 37 °C, 83.2 ± 0.4 U/mg), with optimum pH and temperature of 9.5 (Figure 2B) and 55–60 °C respectively. Nevertheless, the enzyme was active over a broad pH range (pH 6.5–11), in line with the growth of the bacteria in the pH range of 4.5–8.5 [13]. The pH range of the enzyme was broader on the alkaline side than previously reported for the natural enzyme [12]. The notable alkaline tolerance of FspNAMDH agrees with the high ratio of arginine/(arginine + lysine) residues in its sequence (value for this

ratio, 0.55), since ratios above 0.5 characterize alkaline-tolerant enzymes [36].

We were surprised to find a 10–15 °C higher optimum temperature for the activity assay (55–60 °C) than previously reported for the natural enzyme [12], although this may be due to the use of Tris/HCl buffer in the prior assays and of glycine buffer in the present ones. Nevertheless, the enzyme exhibited substantial activity within the temperature range at which *Flavobacterium* sp. 141-8 grows (up to 41 °C) [13]. The use of different buffers is known to influence thermal stability of enzymes even at the same pH [36]. Furthermore, thermofluor assays [34] (Figure 2C and inset thereof) revealed a lower unfolding temperature of FspNAMDH with Tris/HCl (the buffer used in previous studies) than with glycine. With this last buffer, at pH 9.4, unfolding only occurred above 60 °C, in agreement with the full preservation of the activity up to this temperature, particularly since the substrates present in the assay may be expected to induce thermal protection. Actually, the stability of our enzyme in glycine buffer ($T_m = 64$ °C) was similar to that achieved with known protein stabilizers, such as hydroxyectoine 1 M ($T_m = 63$ °C) or ammonium sulfate 1 M ($T_m = 68$ °C) (results not shown), suggesting that glycine itself might have a stabilizing effect.

The enzyme exhibited no activity with mannosamine or with $NADP^+$, thus attesting high specificity for both substrates. The dependence of the activity on the concentrations of both substrates was hyperbolic, with apparent K_m values (0.46 ± 0.02 mM for NAD^+; 0.55 ± 0.01 mM for ManNAc) of the same order or even somewhat lower than those reported earlier [12,14]. Interestingly, the Neu5Ac aldolases, which use ManNAc in the rare aldehyde form (the open form), exhibit much higher K_m values for ManNAc (160–220 mM [35]), suggesting that FspNAMDH utilizes the predominant pyranose form of the sugar.

Crystal structure of NAMDH

Crystals of FspNAMDH in its apo form or bound to ManNAc or NAD^+ diffracted X-rays to 1.9 Å, 2.15 Å and 2.2 Å resolution respectively (Table 1). The sequence identity of 37 % with the hypothetical oxidoreductase of known structure TT0321 (PDB code 2D1Y) (Figure 3), from *T. thermophilus*, led us to successfully use this protein structure for phasing, yielding solutions consisting of one, four and two enzyme homotetramers in the asymmetric unit of the respective crystals of the apo (Table 1, Native) and the ManNAc and NAD^+ complexes.

The FspNAMDH subunit was compact and globular (approximate dimensions, 35 Å×40 Å×50 Å). It presented a typical Rossmann fold architecture with a seven-stranded parallel central open β-sheet (topology, β3-β2-β1-β4-β5-β6-β7) sandwiched between helices α1, α2 and α7 on one side and α3–α5 on the other side (Figures 4A and 4B). Helix α6 is far away and runs obliquely relative to the direction of the β-strands, being a part of a long β6–α7 loop that projects over the C-edge of the central β-sheet (Figure 4A). Whereas in FspNAMDH the β6–α6 connection is folded as a rigid loop, in homologous proteins of known structures, such as TT0321 or *Rhodobacter sphaeroides* sorbitol dehydrogenase (39 % identity; PDB code 1K2W) [37], this connection is folded as an α-helix (Figure 3). An additional interesting feature of the subunit fold was the extended and highly ordered C-tail (residues 260–271) which surrounds the C-terminal part of helix α6, making important contacts with neighbouring subunits, being involved in oligomerization and provision of structural stability to the ManNAc-binding site (Figure 4B).

Four FspNAMDH subunits associate into a compact homotetramer, which presents 222 point group symmetry (Figures 4C–4E), with the three perpendicular 2-fold axes (P, Q and R) defining three different dimers, of which dimer AB (and A'B') (Figures 4C–4E), formed around the Q-axis, exhibits the largest interactions (Q interface, ∼885 Å^2 buried surface per subunit corresponding to 14 % of the subunit surface), mediated by the α4 and α5 helices of both subunits forming a four-helix bundle (Figure 4D and Supplementary Figure S1 at http://www.biochemj.org/bj/462/bj4620499add.htm). In turn, the AB' (or BA') dimer is formed around the P-loop (Figures 4C and 4D) with an interface (P-interface) that buries ∼753 Å^2 per subunit (12 % of the subunit surface). The β-sheets of the two subunits merge at this interface, forming a 14-stranded molecular open concave β-sheet (Figure 4C and Supplementary Figure S1) thanks to non-canonical antiparallel contacts of the β7 strands of both subunits. Helix α6, the C-tail, helix α7 and the C-terminal two turns of helix α5 are also involved in the contacts at this interface. Finally, the AA' (or BB') dimer, formed around the R axis (Figures 4C and 4E), presents a smaller (∼647 A^2 per subunit, ∼10 % of the surface area of the subunit) interface (known as the R-interface) involving helix α6, the C-tail and the β4–α4 and β5–α5 loops. At this interface the C-tail of each subunit is clamped between helix α6 and loops β4–α5 and β5–α6 of the other subunit, stabilizing the tetramer. Interestingly, this diagonal interface, which is also very close to the ManNAc site of the subunit that receives the C-tail of the other subunit, is much more developed in FspNAMDH than in its protein homologues, such as sorbitol dehydrogenase and *Gluconobacter frateurii* L-sorbose reductase (PDB code 3AI3) (Figure 3), which exhibit smaller buried surfaces areas at this interface (only 135 and 297 Å^2 respectively) [37,38]. Otherwise the FspNAMDH fold and architecture are very similar to those of its homologues (all belonging to the SDR family), with low RMSD values for superimposition of Cα carbons of the subunits (one by one) or the entire tetramer. For example, modest RMSD values not exceeding 1.5 Å were obtained for superimposition of the Cα atoms (227–233 atoms) of the FspNAMDH tetramer with the tetramers of TT0321, *R. sphaeroides* sorbitol dehydrogenase [37] or RsGDH (*R. sphaeroides* galactitol dehydrogenase; PDB code 3LQF [39] (Figure 3).

The binding of ManNAc explains the specificity of the enzyme for the *N*-acetyl amino sugar substrate

A large mass of non-protein electron density fitting a ManNAc molecule in partial occupancy (0.7–1, depending on the subunit) was found in the FspNAMDH crystal grown in the presence of ManNAc (Figure 5A), in the same orientation and at an approximately equivalent place than the mannose molecule observed in the structure of *Thermoplasma acidophilum* [AldT (aldohexose dehydrogenase); PDB code 2DTX; another enzyme of the SDR family that exhibits 29 % sequence identity with FspNAMDH] [17] (Figure 5B). The amino sugar is at the bottom of the cleft formed over the C-edge of the β-sheet (Figures 4A, 5C and 5D, and Supplementary Figure S2 at http://www.biochemj.org/bj/462/bj4620499add.htm) by the N-terminal halves of helices α4 and α5 and their connecting loops, on one side, and by helix α6 and its flanking loops β6–α6 and α6–α7 on the other side. Thus the substrate is in a gorge (Figures 4A, 4B, 5C and 5D, and Supplementary Figure S2) which is closed towards β7 by the C-tail of the other subunit of the AA' dimer. This tail contributes to stick both walls of the cleft and thus it

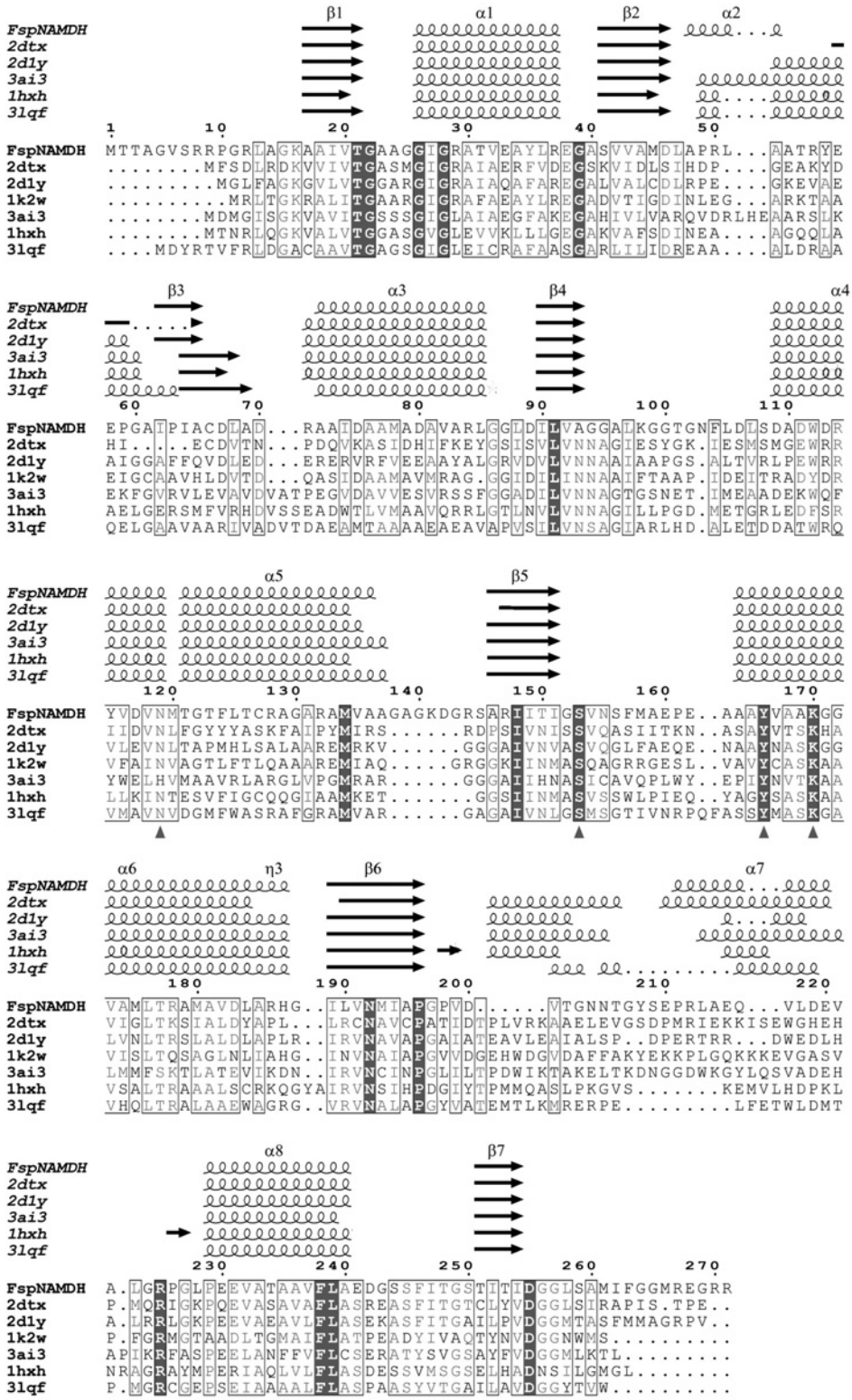

Figure 3 Sequence alignment of FspNAMDH with structurally characterized SDR family homologues

Invariant residues are on a black background. Largely conserved or conservatively replaced residues are boxed. Secondary structure elements (springs, α-helices; arrows, β-strands) are represented above the sequences and are numbered. The four residues of the catalytic tetrad are indicated by arrowheads at the bottom of the sequences. The protein sequences are identified by their PDB codes. 1hxh represents *Comamonas testosterone* 3β/17β-HSD, the other identifiers are described in the text. The Figure was constructed using ESPript [33].

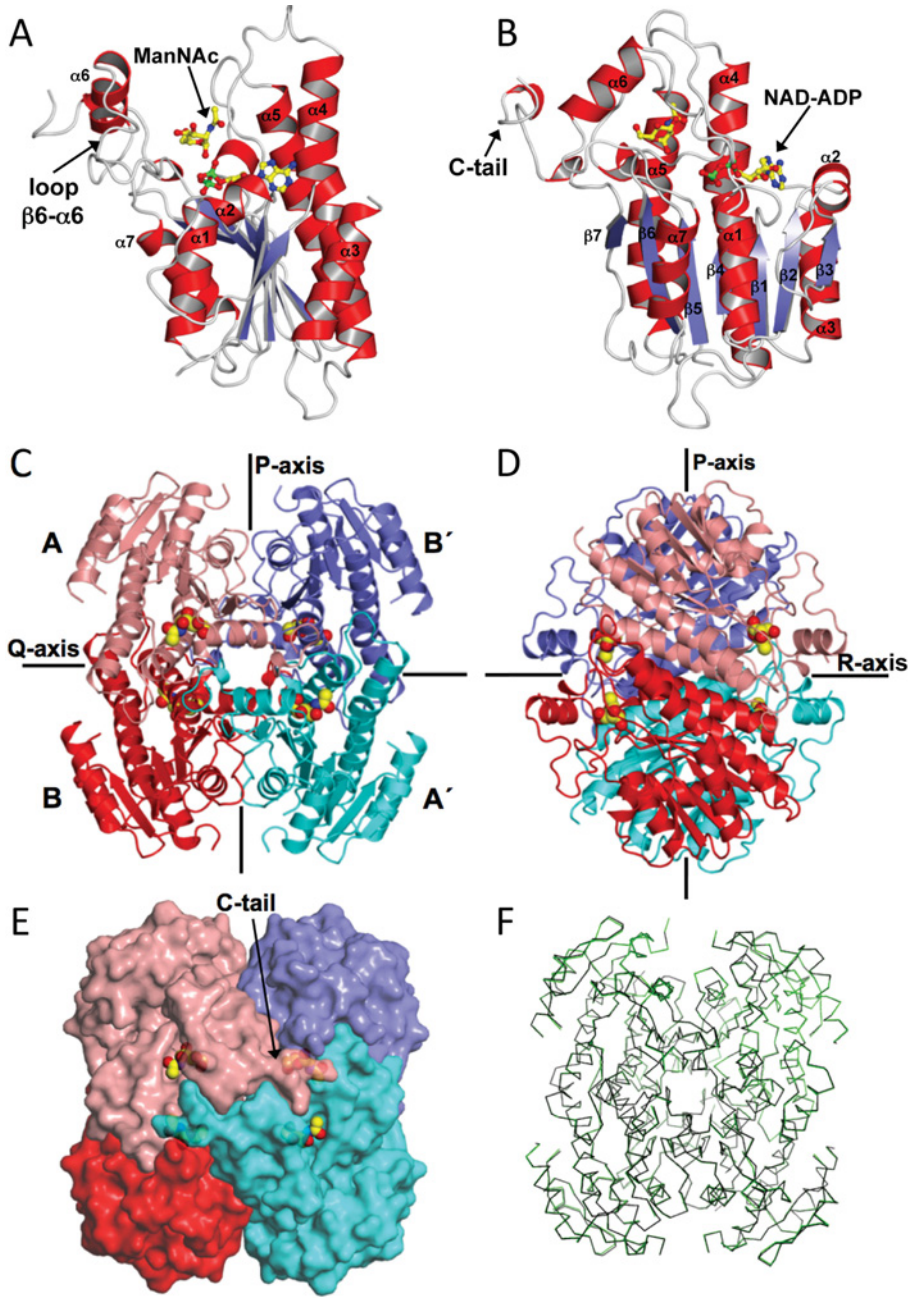

Figure 4 FspNAMDH crystal structure

(**A** and **B**) Orthogonal views of the FspNAMDH subunit with a ManNAc molecule and the ADP moiety of NAD^+ bound (in ball and sticks). The binding of the ADP moiety has been carried out by superimposing the nucleotide from the NAD^+ complex on to the model for the ManNAc complex. Helices, β-strands and loops are coloured red, blue and grey respectively. (**C** and **D**) Orthogonal views of the FspNAMDH tetramer showing the three perpendicular 2-fold axes. The two subunits of each dimer defined by the Q-axis are represented in different shades of either red or blue. (**E**) Surface representation of the tetramer in the same projection as in (**C**) to highlight the C-tail interacting with the neighbour subunit. One bound ManNAc molecule per subunit is represented as spheres. The colour code is as (**C**). (**F**) Superimposition of the Cα trace for the tetramers of FspNAMDH-apo (green) and FspNAMDH–ManNAc (black).

might stabilize the binding site, but it does not provide polar contacts with the bound substrate, although Phe^{263} and Ile^{262} are at average distances of 3.3 and 4 Å respectively from the ManNAc molecule.

In contrast with the lack of polar interactions with the C-tail, the bound ManNAc molecule makes a dense meshwork of polar contacts between all of its polar atoms (except the hydroxy group at C3 of the sugar ring, which is exposed) and protein atoms (Figure 5B). The specificity for the N-acetylated form of the amino sugar is achieved by encasing the *N*-acetamido group in a specific close-binding pocket formed between the side chain of Ala^{163}, which contacts the methyl group of the acetamido substitutent; the carboxylate of Glu^{160}, which hydrogen-bonds the N atom of the acetamido group (as well as the hydroxy group attached to C6 of the hexose); and the Gly^{99} N atom, which is hydrogen bonded to the O atom of the acetamido group. In addition, this group lies flat on the phenolic ring of Tyr^{166}, whereas the phenolic O of this tyrosine is hydrogen-bonded to the hydroxy group of the anomeric C atom. Not surprisingly, the mutation of Tyr^{166} to glutamine or asparagine, which were tested in the present study

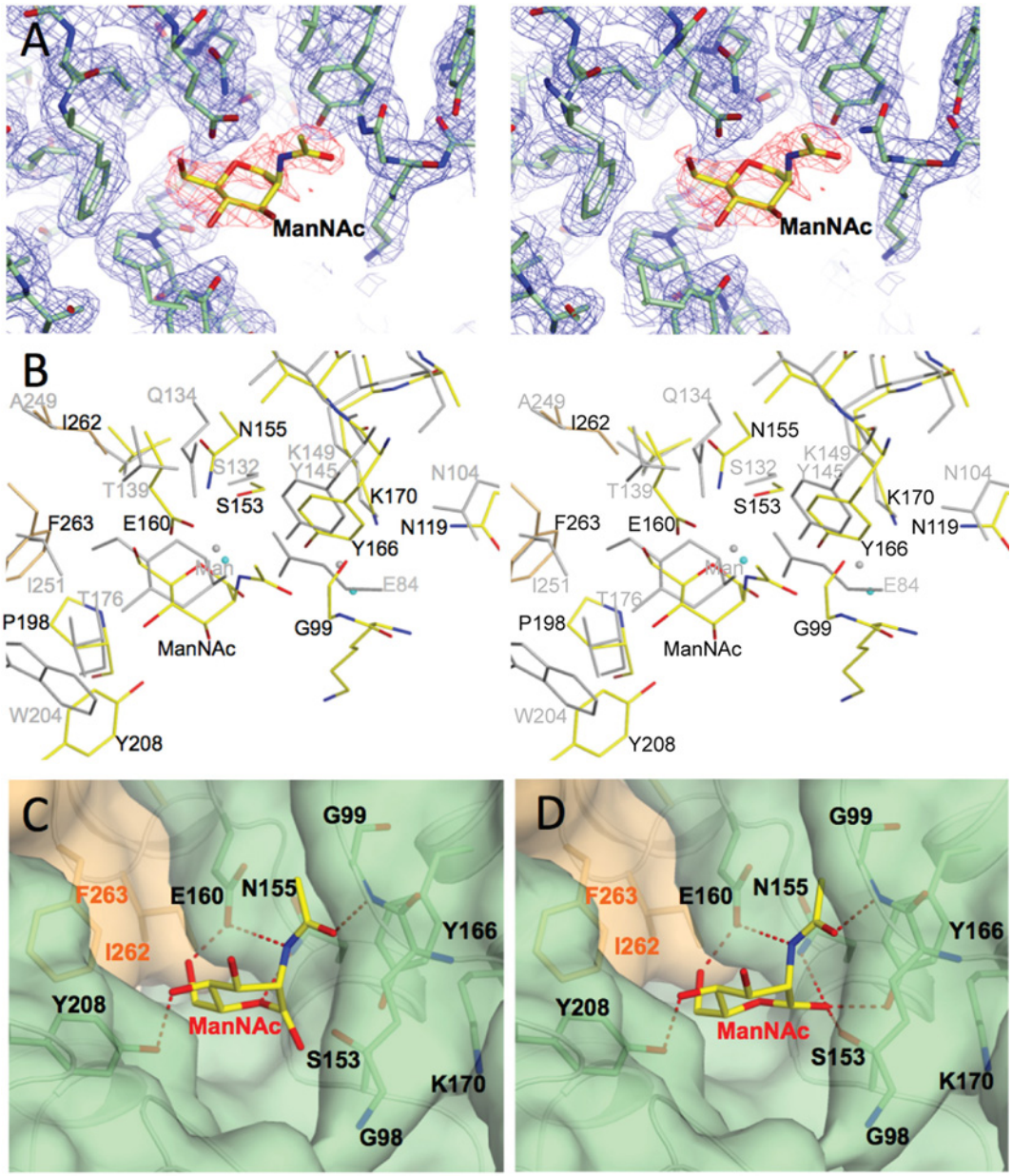

Figure 5 ManNAc-binding site

(**A**) Stereoview of the electron density map around the bound ManNAc molecule (subunit P). The $2F_o - F_c$ electron density map contoured at 1.0 σ is shown as a blue grid and the $F_o - F_c$ omit electron density map for ManNAc, contoured at 2.5 σ, is illustrated as a red grid. The sticks model is coloured in light green and yellow for C atoms of the protein and the ligand respectively. P, N and O atoms are coloured green, blue and red respectively. (**B**) Stereoview of the superimposition of the ManNAc site of FspNAMDH (subunit C; in colour) and the mannose site of AldT (shown in light grey; PDB code 2DTX). (**C** and **D**) View of the substrate gorge in semi-transparent surface representation with one bound ManNAc molecule in α-configuration (**C**) or β-configuration (**D**). Important protein residues are represented in sticks and their secondary structure is shown. The C-tail surface of the adjacent subunit is represented in orange to highlight its nearness to the bound ManNAc substrate.

(Table 2), caused large increases in the apparent K_m value for ManNAc.

As already indicated, a characteristic trait of the FspNAMDH ManNAc site is the replacement of the α-helix found in other members of the SDR immediately after β6, by a loop that is highly structured (Supplementary Figure S3 at http://www.biochemj.org/bj/462/bj4620499add.htm) thanks to interactions mediated by Asp[200]. This rigid loop of FspNAMDH provides Tyr[208], a residue that is hydrogen-bonded to the C4 hydroxy group of the sugar ring, replacing in this function the smaller residues found in other SDR family enzymes (such as Thr[176] of *T. acidophilum* AldT) (Figure 5B). By being bulky and firmly fixed by sandwiching between large hydrophobic side chains of neighbouring residues, Tyr[208] pushes the sugar towards its binding site, helping the acetamido group to fit into its specific binding pocket.

Another finding in our FspNAMDH–ManNAc structure that differs from that in other SDR family members [18] is the inadequate conformation of the ManNAc molecule in some of the subunits for enabling its interaction with the catalytic residues (see below) Ser[153] and Tyr[166]. This is due to the showing of bound ManNAc predominantly in the α-configuration of its anomeric

Table 2 Effects of mutations affecting the putative catalytic tetrad

Variant	K_m^{ManNAc} (mM)	k_{cat} (s^{-1})	k_{cat}/K_m ($mM^{-1}\cdot s^{-1}$)
Wild-type	0.55 ± 0.01	218.9 ± 0.1	397.9
Y166N	11.4 ± 0.1	9.9 ± 0.2	0.9
Y166Q	108.0 ± 0.1	26.5 ± 0.1	0.2
S153T	2.5 ± 0.2	37.3 ± 0.3	14.9
N119A	5.5 ± 0.1	15.6 ± 0.1	2.8
N119S	4.0 ± 0.2	48.4 ± 0.1	12.1
K170R	1.12 ± 0.02	8.5 ± 0.3	7.6

carbon (Figure 5C). In fact, both anomers coexist with different occupations, with predominance of occupancy of the β-anomer in subunits D and L. Correspondingly, in these subunits the hydroxy group on the C1 of the sugar was able to interact with residues Ser[153] and Tyr[166] and with Asn[155] (Figure 5D), strongly suggesting that the β-anomer is the active form of the substrate for proton transfer to Tyr[166]. The fact that both anomers coexist with different occupations indicates that the enzyme does not exhibit a high selectivity for one or the other anomer.

ManNAc binding does not appear to induce important conformational changes, as reflected in the low RMSD values (results not shown) obtained when the structure of the ManNAc form is superimposed with that of the ligand-free form (Figure 4F). In fact, the residues at the substrate site are well aligned for substrate binding even in the substrate-free from of the enzyme, with only small movements (<0.5 Å) occurring with some side chains. The most flexible region of the enzyme is the β4–α4 loop, where movements of up to 2 Å could be observed by comparing different subunits in the various crystals (results not shown).

NAD^+ binding

Non-protein electron density interpreted to correspond to the ADP moiety of NAD^+ was patent in the crystals grown in the presence of NAD^+ (Figure 6A), at the same position observed in AldT (Figure 6B), in a deep cleft over the β-sheet C-edge at the N-terminal half of the subunit (Supplementary Figure S2). The characteristic Rossmann-fold dinucleotide cofactor binding motif consensus sequence TGXXXGXG [18], starting at Thr[21] (Figure 3), is found at the ADP subsite of the NAD^+ site, with the ADP phosphate groups hydrogen bonded to the N atoms of Gly[26] and Ile[27], within this motif. Other NAD^+-recognizing residues are also highly conserved, as in other SDR family enzymes, as can be seen when the NAD^+ sites of FspNAMDH and AldT are compared (Figure 6B). The purine interacts with Asp[67] (Asp[53] in AldT) and with the main chain N atom of Leu[68] (Val[54] in AldT), and the ring of the base lies flat over the hydrophobic side chains of Val[118] (Val[103] in AldT) and Leu[68] (Val[54] in AldT) (Figure 6C). Both ribose hydroxy groups are anchored on the protein by bonds with the side chains of Asp[46] and Arg[50]. The hemiacetalic O atom interacts with the N atom of Ala[96] (Gly[82] in AldT).

Although the nicotinamide moiety of NAD^+ was not visible, possibly because it requires the binding of the second substrate for good fixation, comparison with AldT suggests that the site has the same conformation and space to accommodate this part of the dinucleotide as in AldT (Figure 6B). Thus AldT residues Lys[149] and Tyr[145], which bind to the nicotinamide ribose moiety, align with Lys[170] and Tyr[166] of FspNAMDH (Figure 6B). In fact, a water molecule located at the position expected for the hydroxy group of the ribose mimics the interaction with Lys[170] and Tyr[166] in two subunits (G and H) of the FspNAMDH–NAD complex (Figure 6B).

Similarly to ManNAc binding, NAD^+ binding did not trigger important conformational changes, given the very small RMSD values (not exceeding 0.4 Å) for the superimposition of the subunits or even of the entire tetramers from the different crystals, irrespective of whether one or the other substrate was or was not bound. Again, the ligand-free form revealed essentially the same conformation for the cofactor site with minor side chain rearrangements in comparison with the NAD^+-bound form (results not shown).

The proton relay tetrad of FspNAMDH

The oxido-reduction reaction catalysed by the enzymes of the SDR family is believed to rely on the existence of a proton relay mechanism involving a catalytic Asn-Ser-Tyr-Lys tetrad, in which the serine and tyrosine resides play critical roles for activating the O/OH group of the substrate that is the subject of the reaction, and the lysine and the asparagine play proton relay roles, supplying or removing protons depending on the direction of the reaction and ultimately transferring these to solvent molecules [21]. On the basis of sequence comparisons and because of their positions in the enzyme active centre, we identify in FspNAMDH the invariant Tyr[166], Ser[153] and Lys[170], and the nearly invariant Asn[119] (Figure 3), as the four members of this catalytic tetrad, where the tyrosine and serine residues are shown by the structure to interact with the hydroxy group of the anomeric carbon in the subunits in which this carbon is in the β configuration. The involvement of Lys[170] and Asn[119] in the proton relay system is well supported by their position relative to the purported site of the ribose of the nicotinamide ribosyl moiety of the NAD^+, and also because they are well placed around an intraenzymatic solvent reservoir hosting five water molecules that should act as a proton source/proton sink (Figure 7). Four of the five water molecules in that reservoir are conserved in equivalent positions in the corresponding reservoir identified in 3β/17β-HSD (3β/17β-hydroxysteroid dehydrogenase) [21]. This water-filled hydrophilic cavity is surrounded by polar groups provided by conserved amino acids, which include the already mentioned Lys[170] and Asn[119], and also Thr[21] and Thr[123], all of which line the reservoir with their polar side chains, and Ala[93], Gly[95] and Ile[151], lining it with their carbonyl main-chain groups, in this way stabilizing this water-filled cavity and also facilitating proton transfer among them, as reported for 3β/17β-HSD [21].

In further support of the identification of Tyr[166], Ser[153], Lys[170] and Asn[119] as the catalytic tetrad of FspNAMDH, site-directed mutagenesis of these residues resulted in drastic losses in apparent k_{cat} (that is, the rate extrapolated at infinite concentration of ManNAc while the NAD concentration was kept at 3 mM) and even in larger losses in catalytic efficiency of the enzyme (the k_{cat}/K_m^{ManNAc} ratio) (Table 2). Even the mild S153T substitution had a large impact, much more serious than observed for a similar substitution in 3β/17β-HSD [21], suggesting that in this case steric clash to accommodate the extra methyl group of the threonine misplaced the hydroxy group of this residue for activation of the sugar hydroxy group. This clash is warranted, given the crowded environment of the Ser[153] side chain in FspNAMDH (results not shown).

Final considerations

The present structural studies fully confirm FspNAMDH as a genuine member of the SDR family, with all the traits

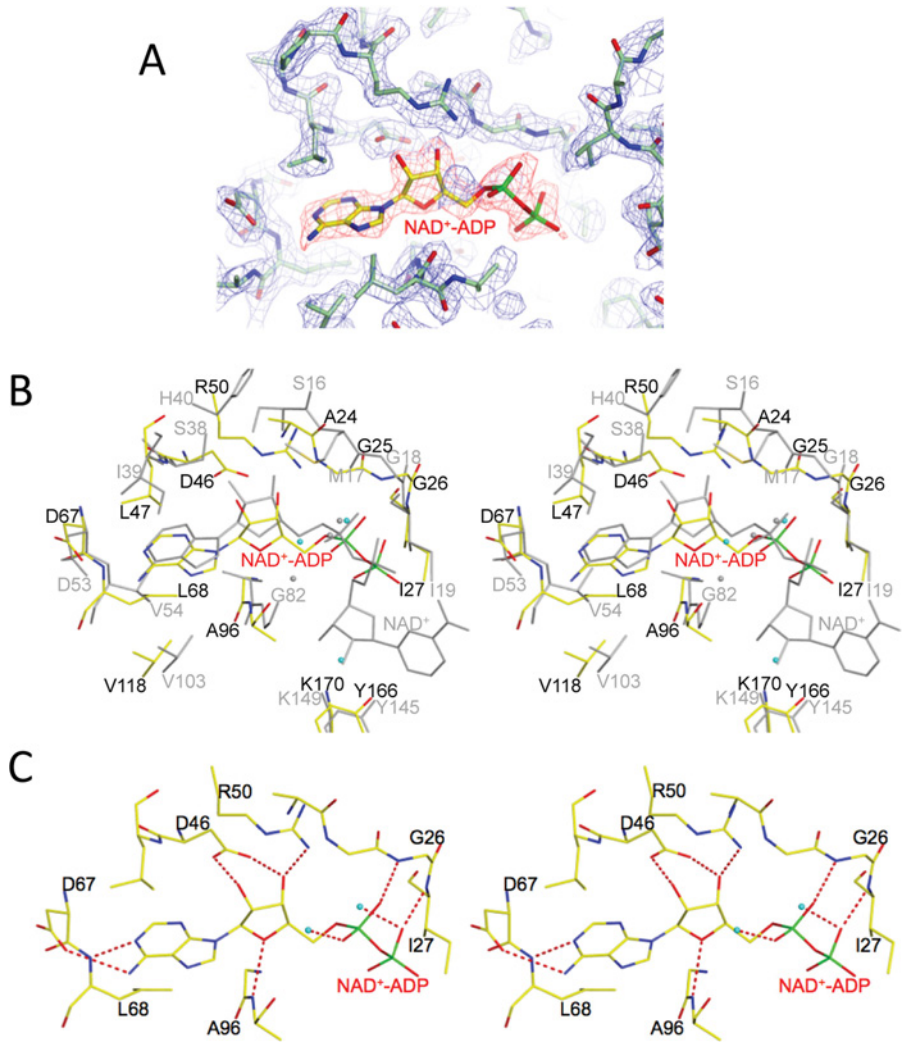

Figure 6 NAD$^+$-binding site

(**A**) Electron density map around the bound NAD$^+$ molecule (subunit H). Relevant residues are shown. The $2F_o - F_c$ electron density map contoured at 1.0 σ is shown as a blue grid and the $F_o - F_c$ omit electron density map around NAD$^+$, contoured at 2.5 σ, is illustrated as a red grid. The sticks model is coloured light green and yellow for C atoms of the protein and ligand respectively. P, N and O atoms are coloured green, blue and red respectively. (**B**) Stereoview in stick representation superimposing the NAD$^+$ molecule and surrounding residues of AldT (light grey) and FspNAMDH subunit H (coloured). (**C**) Stereoview of the cofactor-binding site of FspNAMDH showing the interactions between NAD$^+$ and surrounding residues.

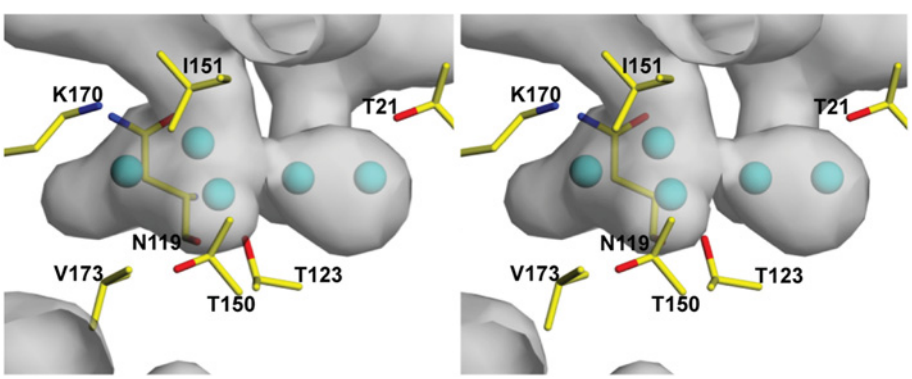

Figure 7 Proton-relay system of FspNAMDH

Surface representation in stereoview showing the hydrophilic pocket with its five enclosed fixed water molecules (cyan spheres). Residues surrounding the pocket are represented in sticks and labelled.

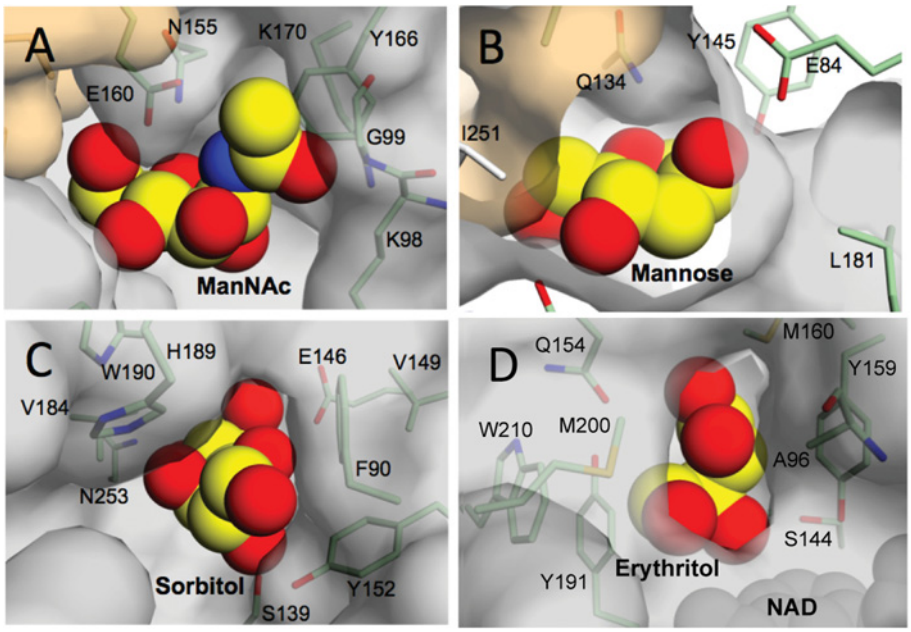

Figure 8 Variability of the substrate site in the SDR family

Comparison of the FspNAMDH site for ManNAc (**A**) with several homologues of the SDR family: the mannose site of AldT (PDB code 2DTX) (**B**); the site of RcSDH (sorbitol dehydrogenase from *R. capsulatus* SB1003) (PDB code 1K2W) with sorbitol modelled (theoretical model PDB 1UZO) (**C**); and the site of RsGDH with erythritol bound (PDB code 3LQF) (**D**). The enzymes are in semi-transparent surface representations, and the substrates (labelled) are shown in spheres representation, to highlight the complementarity with the site and to provide insight on the acetamido group specificity in FspNAMDH. Note that the Glu^{84} of the AldT is replaced in FspNAMDH by Gly^{99}, which has no side chain, leaving space for fitting in the acetamido group. One face of the ManNAc molecule is exposed (**A**), whereas the mannose is completely enclosed (**B**).

for pertaining to it, including fold, architecture, sequence conservation and the existence of a catalytic tetrad that reflects the conservation of the family mechanism for carrying out the NAD^+/NADH-based oxido/reduction reaction. As is customary among members of this family [18], the site for the non-NAD^+ substrate is the one exhibiting the highest specialization, having a structure and residue composition that fully accounts for the specificity of the enzyme for the N-acetylated form of mannosamine, mainly on the basis of the encasing of the acetamido group in a specific binding pocket, and also by using a bulky firmly fixed tyrosine residue (Tyr^{208}) to make contacts with the OH group at C4 of the sugar ring and to push the substrate to having its acetamido group into its highly complementary encasement. Since residue Tyr^{208} is not conserved across the SDR family (Figure 3), it may be an identifying sequence trait for annotating genuine NAMDH sequences in genomic databases. In addition, although loop β4–α4 is involved in substrate binding in many enzymes of the SDR family, it plays an important role in limiting the size of the substrate-binding pocket. In FspNAMDH, it hosts a residue without a side chain, Gly^{99}, instead of a bulky side chain that would have prevented the binding of the acetamido group of the ManNAc, as in many other enzymes of this family (Figure 8A). In this respect, Gly^{99} also appears to be a very important residue for determining the specificity of the enzyme for ManNAc, and since it is not conserved in other members of the family, it might also be used for helping identification of NAMDH in sequence databases. The importance of this residue in selecting for a substrate is exemplified by the comparison with the structure of AldT, where the glycine is replaced by a bulky glutamate (Glu^{84}) residue, that prevents the access of acetylated mannosamine, endowing the cavity with the optimal size for binding the mannose O2 atom (Figure 8B). Further evidence for the importance of the β4–α4 loop to limit the size of the substrate that can be bound by the enzyme is provided by the structure of *R. sphaeroides* sorbitol dehydrogenase, in which the side chain of Phe^{90} also reduces the space available for the substrate to the size of an open sugar (sorbitol) [3] (Figures 8C). In addition to the role of the β4–α4 loop, the substrate site can be limited using other strategies as reported in RsGDH [39]. In this enzyme the substrate site is divided into two regions: a smaller and a larger one, allowing the binding of asymmetric substrates composed by a small and a large substituent, and favouring the binding of linear forms instead of cyclic ones (Figures 8D). The presence of large substituents is allowed thanks to the presence of an alanine residue (Ala^{96}) at the β4–α4 loop, whereas the opposite side of the site is limited by a hydrophobic cushion composed by bulky side chains (Tyr^{191} and Trp^{210}). The absence of this cushion in FspNAMDH and the substitution of the alanine residue in the β4–α4 loop for glycine enlarges the site allowing the fitting of a substrate with larger substituents. Thus it appears clear that the β4–α4 loop represents a key adaptive sequence for expanding/restricting the substrate-binding site in the SDR family and contributes importantly to the specificity of each enzyme.

AUTHOR CONTRIBUTION

Agustín Sola-Carvajal generated the constructs, produced the protein and together, with Francisco García-Carmona, carried out the biochemical studies. Fernando Gil-Ortiz carried out the crystallization studies as well as the analysis and interpretation of the structural data. Vicente Rubio and Álvaro Sánchez-Ferrer directed the work, analysed the results and, together with Fernando Gil-Ortiz and Agustín Sola-Carvajal, wrote the paper.

ACKNOWLEDGEMENTS

We thank the ESRF and Diamond Light Source synchrotron's staff for data collection assistance and the EU and European Molecular Biology Laboratory for funding synchrotron visits.

FUNDING

This study was supported by the Spanish Ministry for Science [grant number MINECO-FEDER BIO2010-22225-C02-01], the Fundación Séneca ('Programa de Ayuda a Grupos de Excelencia de la Región de Murcia', 04541/GERM/06, Plan Regional de Ciencia y Tecnología 2007–2010), the Spanish Ministry of Economy and Innovation [grant number BFU2011-30407] and the Valencian Government [grant number Prometeo/2009/051]. A.S.-C. received a predoctoral research grant from the above project of Grupos de Excelencia de la Región de Murcia. Synchrotron visits were funded by the European Community's Seventh Framework Programme (FP7/2007–2013) under BioStruct-X [grant agreement 283570].

REFERENCES

1 Varki, A. and Schauer, R. (2009) Sialic acids. In Essentials of Glycobiology (Varki, A., Cummings, R. D., Esko, J. D., Freeze, H. H., Stanley, P., Bertozzi, C. R., Hart, G. W. and Etzler, M. E., eds), Chaper 14, Cold Spring Harbor Press, Cold Spring Harbor, NY

2 Hayakawa, K., De Felice, C., Watanabe, T., Tanaka, T., Iinuma, K., Nihei, K., Higuchi, S., Ezoe, T., Hibi, I. and Kurosawa, K. (1993) Determination of free *N*-acetylneuraminic acid in human body fluids by high-performance liquid chromatography with fluorimetric detection. J. Chromatogr. **620**, 25–31 CrossRef PubMed

3 Narayanan, S. (1994) Sialic acid as a tumor marker. Ann. Clin. Lab. Sci. **24**, 376–384 PubMed

4 Regañón, E., Vila, V., Martínez-Sales, V., Vayá, A., Mira, Y., Ferrando, F. and Aznar, J. (2007) Sialic acid is an inflammation marker associated with a history of deep vein thrombosis. Thromb. Res. **119**, 73–78 CrossRef PubMed

5 Crook, M. (1993) The determination of plasma or serum sialic acid. Clin. Biochem. **26**, 31–38 CrossRef PubMed

6 Silver, R. P., Finn, C. W., Vann, W. F., Aaronson, W., Schneerson, R., Kretschmer, P. J. and Garon, C. F. (1981) Molecular cloning of the K1 capsular polysaccharide genes of *E. coli*. Nature **289**, 696–698 CrossRef PubMed

7 Schauer, R. (1985) Sialic acids and their roles as biological masks. Trends Biochem. Sci. **10**, 357–360 CrossRef

8 Severi, E., Hood, D. W. and Thomas, G. H. (2007) Sialic acid utilization by bacterial pathogens. Microbiology **153**, 2817–2822 CrossRef PubMed

9 Vimr, E. R., Kalivoda, K. A., Deszo, E. L. and Steenbergen, S. M. (2004) Diversity of microbial sialic acid metabolism. Microbiol. Mol. Biol. Rev. **68**, 132–153 CrossRef PubMed

10 Almagro-Moreno, S. and Boyd, E. F. (2009) Insights into the evolution of sialic acid catabolism among bacteria. BMC Evol. Biol. **9**, 118 CrossRef PubMed

11 Brigham, C., Caughlan, R., Gallegos, R., Dallas, M. B., Godoy, V. G. and Malamy, M. H. (2009) Sialic acid (*N*-acetyl neuraminic acid) utilization by *Bacteroides fragilis* requires a novel N-acetyl mannosamine epimerase. J. Bacteriol. **191**, 3629–3638 CrossRef PubMed

12 Horiuchi, T. and Kurokawa, T. (1988) Purification and properties of *N*-acyl-D-mannosamine dehydrogenase from *Flavobacterium* sp. 141-8. J. Biochem. **104**, 466–471 PubMed

13 Horiuchi, T. and Kurokawa, T. (1990) N-Acetylmannosamine dehydrogenase, process for its production, method for quantitatively analyzing *N*-acetylmannosamine or sialic acid, and kit for the quantitative analysis., U.S. Pat. 4,960,701

14 Yamamoto-Otake, H., Koyama, Y., Horiuchi, T. and Nakano, E. (1991) Cloning, sequencing, and expression of the N-acyl-D-mannosamine dehydrogenase gene from *Flavobacterium* sp. strain 141-8 in *Escherichia coli*. Appl. Environ. Microbiol. **57**, 1418–1422 PubMed

15 Sola-Carvajal, A., García-García, M. I., Sánchez-Carrón, G., García-Carmona, F. and Sánchez-Ferrer, Á. (2012) Functional assignment of gene AAC16202.1 from *Rhodobacter capsulatus* SB1003: new insights into the bacterial SDR sorbitol dehydrogenases family. Biochimie **94**, 2407–2415 CrossRef PubMed

16 Jornvall, H., Persson, B., Krook, M., Atrian, S., Gonzalez-Duarte, R., Jeffery, J. and Ghosh, D. (1995) Short-chain dehydrogenases/reductases (SDR). Biochemistry **34**, 6003–6013 CrossRef PubMed

17 Yasutake, Y., Nishiya, Y., Tamura, N. and Tamura, T. (2007) Structural insights into unique substrate selectivity of *Thermoplasma acidophilum* D-aldohexose dehydrogenase. J. Mol. Biol. **367**, 1034–1046 CrossRef PubMed

18 Kavanagh, K. L., Jornvall, H., Persson, B. and Oppermann, U. (2008) Medium- and short-chain dehydrogenase/reductase gene and protein families: the SDR superfamily: functional and structural diversity within a family of metabolic and regulatory enzymes. Cell. Mol. Life Sci. **65**, 3895–3906 CrossRef PubMed

19 Keller, B., Volkmann, A., Wilckens, T., Moeller, G. and Adamski, J. (2006) Bioinformatic identification and characterization of new members of short-chain dehydrogenase/reductase superfamily. Mol. Cell Endocrinol. **248**, 56–60 CrossRef PubMed

20 Kallberg, Y., Oppermann, U., Jornvall, H. and Persson, B. (2002) Short-chain dehydrogenases/reductases (SDRs). Eur. J. Biochem. **269**, 4409–4417 CrossRef PubMed

21 Filling, C., Berndt, K. D., Benach, J., Knapp, S., Prozorovski, T., Nordling, E., Ladenstein, R., Jornvall, H. and Oppermann, U. (2002) Critical residues for structure and catalysis in short-chain dehydrogenases/reductases. J. Biol. Chem. **277**, 25677–25684 CrossRef PubMed

22 Sola-Carvajal, A., Sánchez-Carrón, G., García-García, M. I., García-Carmona, F. and Sánchez-Ferrer, Á. (2012) Properties of BoAGE2, a second N-acetyl-D-glucosamine 2-epimerase from *Bacteroides ovatus* ATCC 8483. Biochimie **94**, 222–230 CrossRef PubMed

23 Laemmli, U. K. (1970) Cleavage of structural proteins during the assembly of the head of bacteriophage T4. Nature **227**, 680–685 CrossRef PubMed

24 Bradford, M. M. (1976) A rapid and sensitive method for the quantitation of microgram quantities of protein utilizing the principle of protein-dye binding. Anal. Biochem. **72**, 248–254 CrossRef PubMed

25 Ho, S. N., Hunt, H. D., Horton, R. M., Pullen, J. K. and Pease, L. R. (1989) Site-directed mutagenesis by overlap extension using the polymerase chain reaction. Gene **77**, 51–59 CrossRef PubMed

26 Jancarik, J. and Kim, S.-H. (1991) Sparse matrix sampling: a screening method for crystallization of proteins. J. Appl. Crystallog. **24**, 409–411 CrossRef

27 Collaborative Computational Project, Number 4 (1994) The CCP4 suite: programs for protein crystallography. Acta Crystallogr. D Biol. Crystallogr. **50**, 760–763 CrossRef PubMed

28 Kabsch, W. (2010) XDS. Acta Crystallogr. D Biol. Crystallogr. **66**, 125–132 CrossRef PubMed

29 Emsley, P. and Cowtan, K. (2004) Coot: model-building tools for molecular graphics. Acta Crystallogr. D Biol. Crystallogr. **60**, 2126–2132 CrossRef PubMed

30 Painter, J. and Merritt, E. A. (2006) Optimal description of a protein structure in terms of multiple groups undergoing TLS motion. Acta Crystallogr. D Biol. Crystallogr. **62**, 439–450 CrossRef PubMed

31 Laskowski, R. A., MacArthur, M. W., Moss, D. S. and Thornton, J. M. (1993) PROCHECK: a program to check the stereochemical quality of protein structures. J. Appl. Crystallog. **26**, 283–291 CrossRef

32 Krissinel, E. and Henrick, K. (2004) Secondary-structure matching (SSM), a new tool for fast protein structure alignment in three dimensions. Acta Crystallogr. D Biol. Crystallogr. **60**, 2256–2268 CrossRef PubMed

33 Gouet, P., Courcelle, E., Stuart, D. I. and Metoz, F. (1999) ESPript: analysis of multiple sequence alignments in PostScript. Bioinformatics **15**, 305–308 CrossRef PubMed

34 Niesen, F. H., Berglund, H. and Vedadi, M. (2007) The use of differential scanning fluorimetry to detect ligand interactions that promote protein stability. Nat. Protoc. **2**, 2212–2221 CrossRef PubMed

35 Sanchez-Carrión, G., García-García, M. I., López-Rodríguez, A. B., Jiménez-García, S., Sola-Carvajal, A., García-Carmona, F. and Sánchez-Ferrer, A. (2011) Molecular characterization of a novel N-acetylneuraminate lyase from *Lactobacillus plantarum* WCFS1. Appl. Environ. Microbiol. **77**, 2471–2478 CrossRef PubMed

36 Deng, A., Wu, J., Zhang, G. and Wen, T. (2011) Molecular and structural characterization of a surfactant-stable high-alkaline protease AprB with a novel structural feature unique to subtilisin family. Biochimie **93**, 783–791 CrossRef PubMed

37 Philippsen, A., Schirmer, T., Stein, M. A., Giffhorn, F. and Stetefeld, J. (2005) Structure of zinc-independent sorbitol dehydrogenase from *Rhodobacter sphaeroides* at 2.4 Å resolution. Acta Crystallogr. D Biol. Crystallogr. **61**, 374–379 CrossRef PubMed

38 Kubota, K., Nagata, K., Okai, M., Miyazono, K., Soemphol, W., Ohtsuka, J., Yamamura, A., Saichana, N., Toyama, H., Matsushita, K. and Tanokura, M. (2011) The crystal structure of L-sorbose reductase from *Gluconobacter frateurii* complexed with NADPH and L-sorbose. J. Mol. Biol. **407**, 543–555 CrossRef PubMed

39 Carius, Y., Christian, H., Faust, A., Zander, U., Klink, B. U., Kornberger, P., Kohring, G.-W., Giffhorn, F. and Scheidig, A. J. (2010) Structural insight into substrate differentiation of the sugar-metabolizing enzyme galactitol dehydrogenase from *Rhodobacter sphaeroides* D. J. Biol. Chem. **285**, 20006–20014 CrossRef PubMed

Received 27 February 2014/26 June 2014; accepted 27 June 2014
Published as BJ Immediate Publication 27 June 2014, doi:10.1042/BJ20140266

Biochem. J. (2014) **462**, 499–511 (Printed in Great Britain) doi:10.1042/BJ20140266

online data

SUPPLEMENTARY ONLINE DATA

Crystal structures and functional studies clarify substrate selectivity and catalytic residues for the unique orphan enzyme *N*-acetyl-D-mannosamine dehydrogenase

Agustín SOLA-CARVAJAL*[1], Fernando GIL-ORTIZ†‡[1], Francisco GARCÍA-CARMONA*, Vicente RUBIO†[2] and Álvaro SÁNCHEZ-FERRER*§[2]

*Department of Biochemistry and Molecular Biology-A, Faculty of Biology, Regional Campus of International Excellence "*Campus Mare Nostrum*", University of Murcia, Campus Espinardo, E-30100 Murcia, Spain
†Instituto de Biomedicina de Valencia-Consejo Superior de Investigaciones Científicas (IBV-CSIC) and Centro de Investigación Biomédica en Red de Enfermedades Raras (CIBERER-ISCIII), Valencia, Spain
‡CELLS-ALBA Synchrotron Light Source, 08290 Barcelona, Spain
§Murcia Biomedical Research Institute (IMIB-Arrixaca), 30120 Murcia, Spain

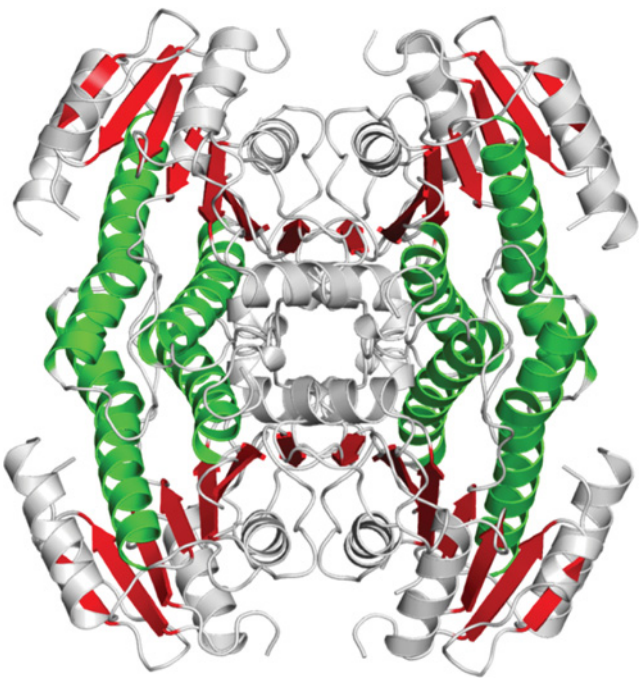

Figure S1 The FspNAMDH tetramer

The view is along the Q-axis. The four helices at each bundle at the junctions between the two subunits of both dimers formed around the Q-axis are shown in green. The 14-stranded molecular β-sheets of the two dimers formed around the P-axis are coloured red.

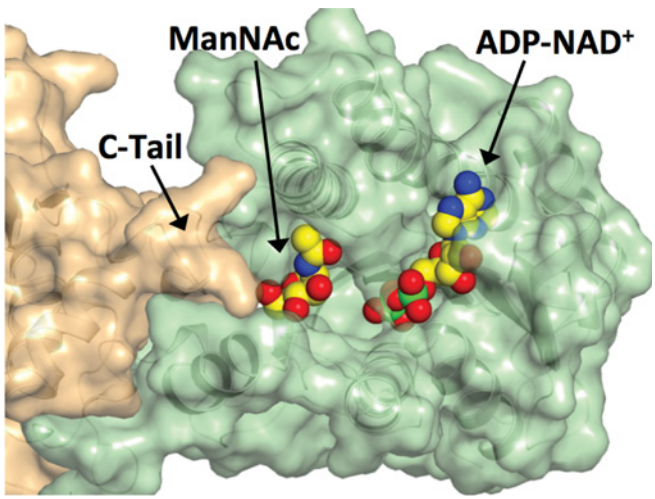

Figure S2 General view of the FspNAMDH binding sites

View of the substrate sites of FspNAMDH in semi-transparent surface representation. The secondary structure is shown. The ManNAc and the modelled (by superimposition of the NAD^+ complex) ADP portion of NAD^+ are represented in spheres. The C-tail surface of the adjacent subunit is represented in orange.

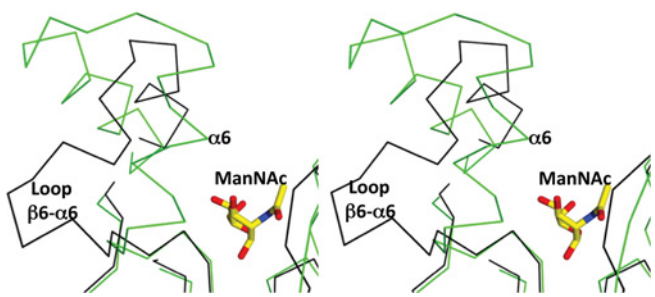

Figure S3 Helix α6 is substituted by a loop in FspNAMDH

Stereoview of the superimposition (in Cα trace) of FspNAMDH (black) and AldT (green; PDB code 2DTX) substrate-binding sites. ManNAc is shown in ball and stick representation.

[1] These authors contributed equally to this work.
[2] Correspondence may be addressed to either of these authors (rubio@ibv.csic.es or alvaro@um.es).

The co-ordinates and structure factors for the FspNAMDH-apo, FspNAMDH–ManNAc and FspNAMDH–NAD crystal structures have been deposited in the PDB under codes 4CR6, 4CR7 and 4CR8 respectively.

Table S1 Oligonucleotides used for site-directed mutagenesis of FspNAMDH

The mutated codons are underlined.

Oligonucleotide	Sequence 5′–3′
N119A-forward	CGCTATGTCGACGTCGCCATGACCGGCACCTTC
N119A-reverse	GAAGGTGCCGGTCATGGCGACGTCGACATAGCG
N119S-forward	CCGCTATGTCGACGTCTCCATGACCGGCACCTTCC
N119S-reverse	GGAAGGTGCCGGTCATGGAGACGTCGACATAGCGG
S153T-forward	CGCATCATCACCATCGGCACCGTCAATTCCTTCATGGCC
S153Thr-Reverse	GGCCATGAAGGAATTGACGGTGCCGATGGTGATGATGCG
Y166N-forward	GGAGGCGGCCGCCAATGTCGCGGCCAAGG
Y166N-reverse	CCTTGGCCGCGACATTGGCGGCCGCCTCC
Y166Q-forward	GGAGGCGGCCGCCCAAGTCGCGGCCAAGG
Y166Q-reverse	CCTTGGCCGCGACTTGGGCGGCCGCCTCC
K170R-forward	CTATGTCGCGGCCCGGGGCGGCGTCGCCA
K170R-reverse	TGGCGACGCCGCCCCGGGCCGCGACATAG

Received 27 February 2014/26 June 2014; accepted 27 June 2014
Published as BJ Immediate Publication 27 June 2014, doi:10.1042/BJ20140266